

Electronic Supplementary Information (ESI) for

Construction of C@MoS₂@C Sandwiched Heterostructure for
Accelerating pH-Universal Hydrogen Evolution Reaction

Yan Mei,^a Ting-Ting Li,^{*a} Jinjie Qian,^{*b} Hongwei Li,^a Miao Wu,^a
Yue-Qing Zheng^{*a}

^aSchool of Materials Science and Chemical Engineering, Ningbo University, Ningbo,
315211, China;

^bCollege of Chemistry and Materials Engineering, Wenzhou University, Wenzhou,
325000, China.

Experimental section

Materials and reagents

Ferric chloride hexahydrate ($\text{FeCl}_3 \cdot 6\text{H}_2\text{O}$), methyl orange, pyrrole monomer, diethylenetriamine, sodium molybdate ($\text{Na}_2\text{MoO}_4 \cdot 2\text{H}_2\text{O}$), thiourea ($\text{CH}_4\text{N}_2\text{S}$), glucose, Pt/C (10%), concentrated sulfuric acid (H_2SO_4), concentrated nitric acid (HNO_3), sodium phosphate monobasic (NaH_2PO_4), sodium phosphate dibasic (Na_2HPO_4) and potassium hydroxide (KOH) were commercially obtained from Shanghai Aladdin Co., Ltd without further purification. All the aqueous solutions were prepared using Milli-Q ultrapure water ($>18 \text{ M}\Omega$) unless stated otherwise. Carbon cloth (CC) was purchased from Taiwan CeTech Co., Ltd. For improving the hydrophilicity, CC was treated by the mixed solution of 10 wt% HNO_3 and 10 wt% H_2SO_4 with a volume ratio of 3:1.

Preparation of polypyrrole-derived carbon nanotube (PCN)

Firstly, 0.4 g of $\text{FeCl}_3 \cdot 6\text{H}_2\text{O}$ was added into 30 mL of aqueous solution with methyl orange concentration of 5 mmol L^{-1} under vigorous stirring. And then, 150 μL of pyrrole monomer was added into the above suspension and reacted for 24 h under ambient conditions. The formed black precipitate was collected by filtration and washed repeatedly with distilled water and ethanol, and dried in a vacuum oven overnight. Finally, the black powder was annealed at $650 \text{ }^\circ\text{C}$ for 2 h in a tube furnace with N_2 atmosphere to obtain PCN.

Preparation of PCN@MoS₂@C sandwiched heterostructure

30 mg of PCN was dispersed into deionized water by ultrasonication for 1 h to obtain the suspension, and 5 mL of DETA was added into the suspension. The mixture was stirred for 1 h to obtain a homogeneous solution. And then, 0.2 g of $\text{Na}_2\text{MoO}_4 \cdot 2\text{H}_2\text{O}$, 0.4 g of thiourea and 50 mg of glucose were successively added into the solution and further reacted for another 1 h. The solution was transferred to a Teflon-lined stainless steel autoclave and treated at $200 \text{ }^\circ\text{C}$ for 24 h in an oven. After that, the obtained precipitate was collected by centrifugation, washed repeatedly with distilled water and ethanol, and dried in a vacuum oven overnight. For comparison,

two other PCN@MoS₂@C samples with thinner or thicker carbon shells were prepared by changing the concentration of glucose.

The counterpart PCN@MoS₂ product was prepared via the same procedure but without the addition of DETA and glucose.

Preparation of working electrode

The working electrode of PCN, PCN@MoS₂, PCN@MoS₂@C or commercial Pt/C with a mass loading of 40 μg cm⁻² on carbon cloth was prepared via a drop-casting approach with the assistance of Nafion solution. Firstly, 4 mg of sample was dispersed into the mixed solution containing 0.9 mL of isopropanol and 0.1 mL Nafion solution (5 %) by ultrasonication for 30 min to obtain the homogeneous catalyst ink. And then 10 μL of catalyst ink was dropped onto the carbon cloth (1 × 1 cm²). Finally, the resulting working electrode was dried under ambient conditions overnight.

Physicochemical characterizations

Powder X-ray diffraction (XRD) analysis was performed on a Bruker AXS D8 Advance X-ray diffractometer with Cu Kα radiation ($\lambda = 1.5046 \text{ \AA}$) in the 2θ range of 10 to 80° with a scan rate of 6° min⁻¹. The morphologies and related energy-dispersive X-ray (EDX) elemental mapping of samples were recorded using a field emission scanning electron microscope (FE-SEM, Hitachi S-4800) operated at an accelerating voltage of 20 kV. Transmission electron microscope (TEM), high-resolution TEM (HR-TEM) images were obtained on a JEOL JEM-2100 electron microscope with an accelerating voltage of 200 kV. Raman spectra were collected from a Renishaw inVia Raman spectrometer with excitation from the 532 nm line of an Ar ion laser. X-ray photoelectron spectroscopy (XPS) measurements were carried out on an ESCALAB 250 instrument with Mg as the excitation source, the binding energies (BE) were corrected by referencing the C1s peak at 284.6 eV.

Electrochemical measurements

All electrochemical measurements were carried out on a CHI 760 electrochemical workstation with a standard three-electrode cell under ambient conditions. PCN, PCN@MoS₂, PCN@MoS₂@C and Pt/C powder catalysts were prepared as the

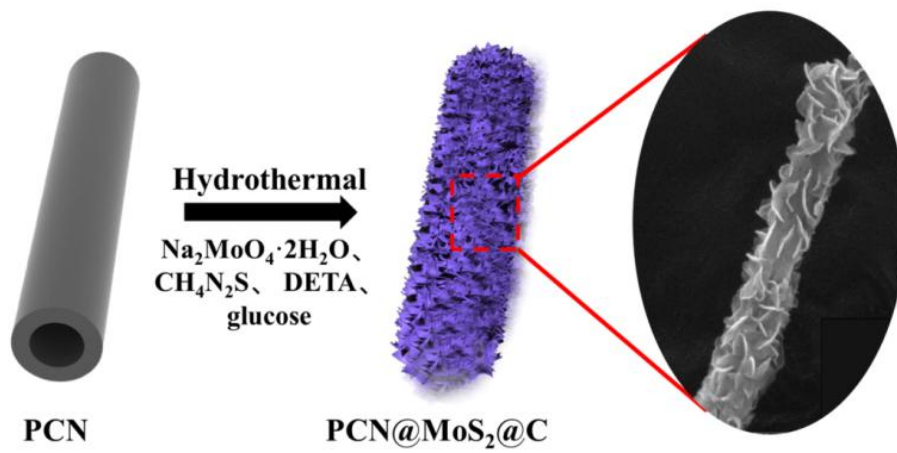
homogeneous inks loading onto CC ($1 \times 1 \text{ cm}^2$) with a mass loading of $40 \mu\text{g cm}^{-2}$ as the working electrode. The graphite rod was used as the counter electrode. In acidic ($0.5 \text{ M H}_2\text{SO}_4$ solution) or neutral (0.1 M phosphate buffer solution) electrolyte, a saturated calomel electrode (SCE) was used as the reference electrode and it was replaced by a Hg/HgO (1 M KOH) electrode in alkaline solution. All potentials recorded in this literature were corrected to the reversible hydrogen electrode (RHE) scale based on the following equation.

$$E (\text{V vs. RHE}) = E (\text{V vs. SCE}) + 0.0592 \times \text{pH} + 0.224 \quad (\text{Eq. S1})$$

$$E (\text{V vs. RHE}) = E (\text{V vs. Hg/HgO}) + 0.0592 \times \text{pH} + 0.099 \quad (\text{Eq. S2})$$

As a pH universal HER catalyst, the catalytic activity of each catalyst was evaluated by linear sweep voltammetry (LSV) and the scan rate of LSV was fixed to 5 mV s^{-1} . All polarization plots were corrected with 80 % iR compensation. Tafel plots were fitted from the corresponding polarization plots. The stability of each sample was assessed by chronopotentiometry or chronoamperometry. Double layer capacitance (C_{dl}) was estimated by cyclic voltammetry (CV) at various scan rates ($10, 20, 40, 60, 80$ and 100 mV s^{-1}) in the potential region of $-0.1 \sim 0 \text{ V vs. RHE}$. The electrochemical surface area (ECSA) of each sample is calculated according to Eq. S3. Electrochemical impedance spectroscopy (EIS) was carried out at -0.5 V vs. RHE over a frequency range from 100 kHz to 0.01 Hz at the amplitude of the sinusoidal voltage of 5 mV . The amount of produced H_2 was quantified by gas chromatography (carrier gas: N_2 ; chromatographic column: 5 \AA molecular sieve column; detector: thermal conductivity detector). The theoretical amount of H_2 was determined by dividing the recorded charge by $2F$ ($F = 96500 \text{ C mol}^{-1}$).

$$A_{\text{ECSA}} = C_{dl}/40 \mu\text{F cm}^{-2} \text{ per cm}_{\text{ECSA}}^2 \quad (\text{Eq. S3})$$



Scheme S1. Synthesis scheme for PCN@MoS₂@C sandwiched heterostructure.

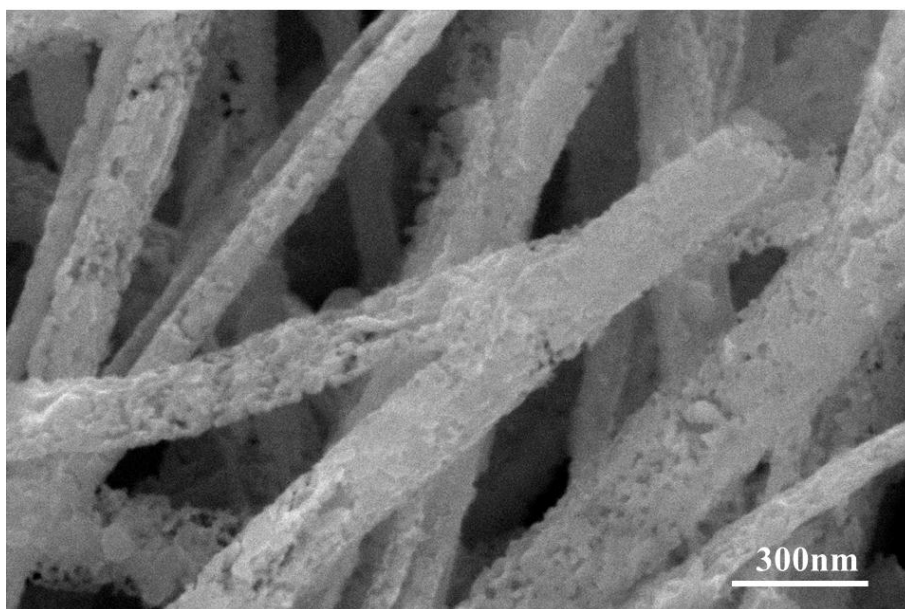


Fig. S1 SEM image of PCN.

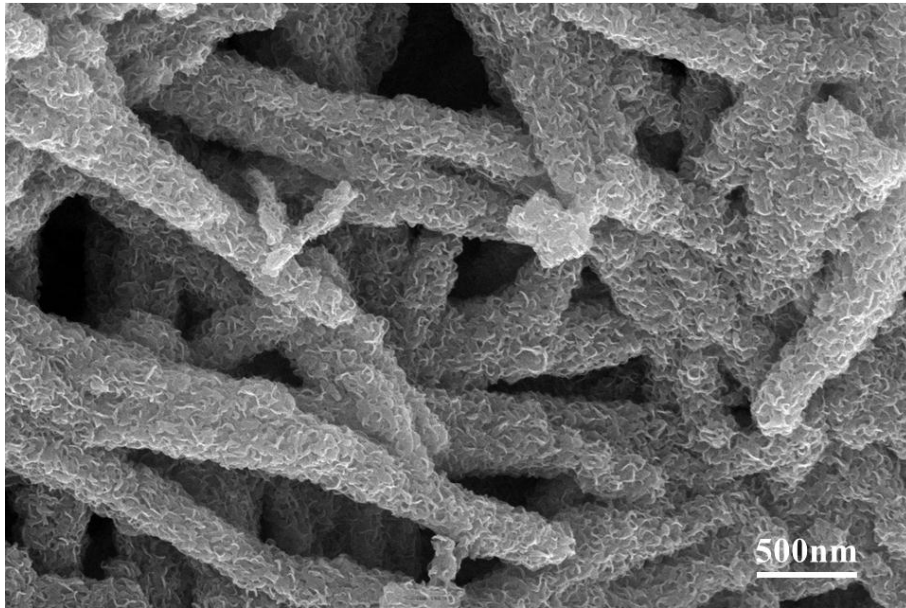


Fig. S2 SEM image of PCN@MoS₂.

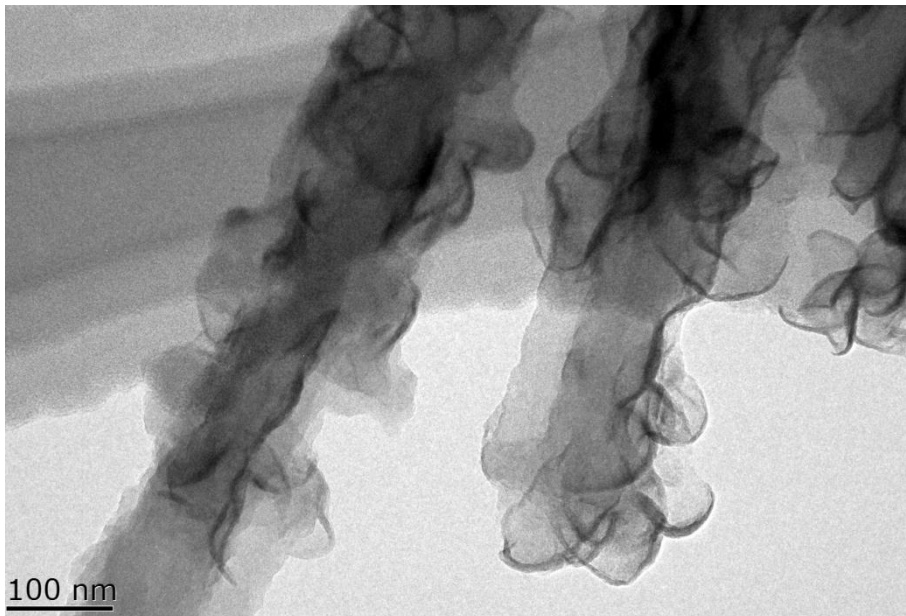
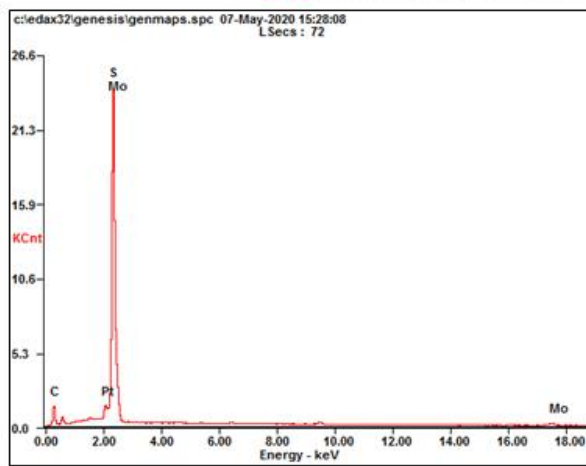
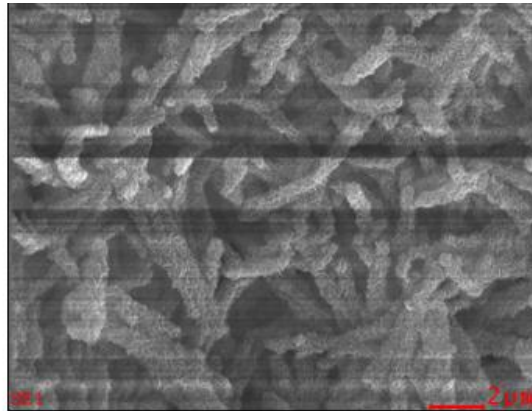


Fig. S3 TEM image of PCN@MoS₂.



<i>Element</i>	<i>Wt%</i>	<i>At%</i>
<i>-CK</i>	44.69	78.86
<i>-SK</i>	20.25	13.39
<i>-MoK</i>	35.06	07.75
<i>Matrix</i>	Correction	ZAF

Fig. S4 EDX elemental spectrum of PCN@MoS₂@C.

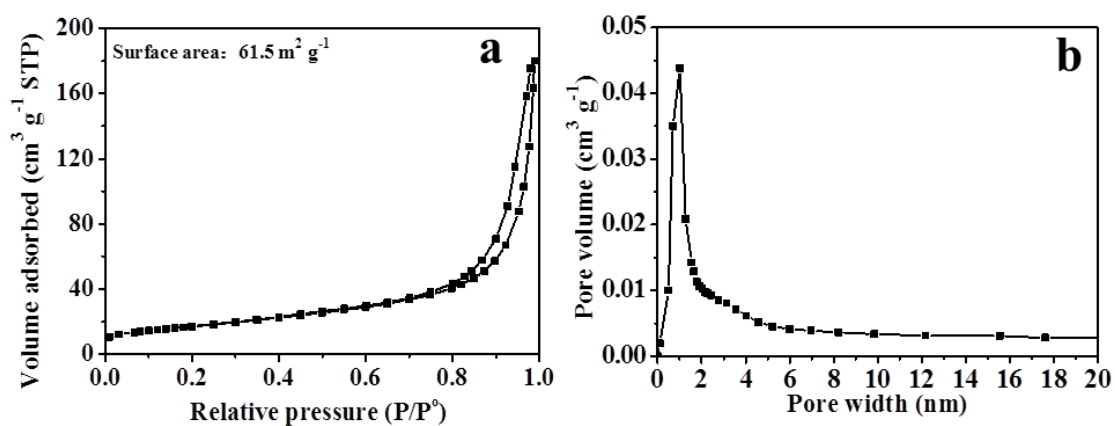


Fig. S5 (a) Nitrogen adsorption/desorption isotherm and (b) BJH pore size distribution of PCN@MoS₂@C.

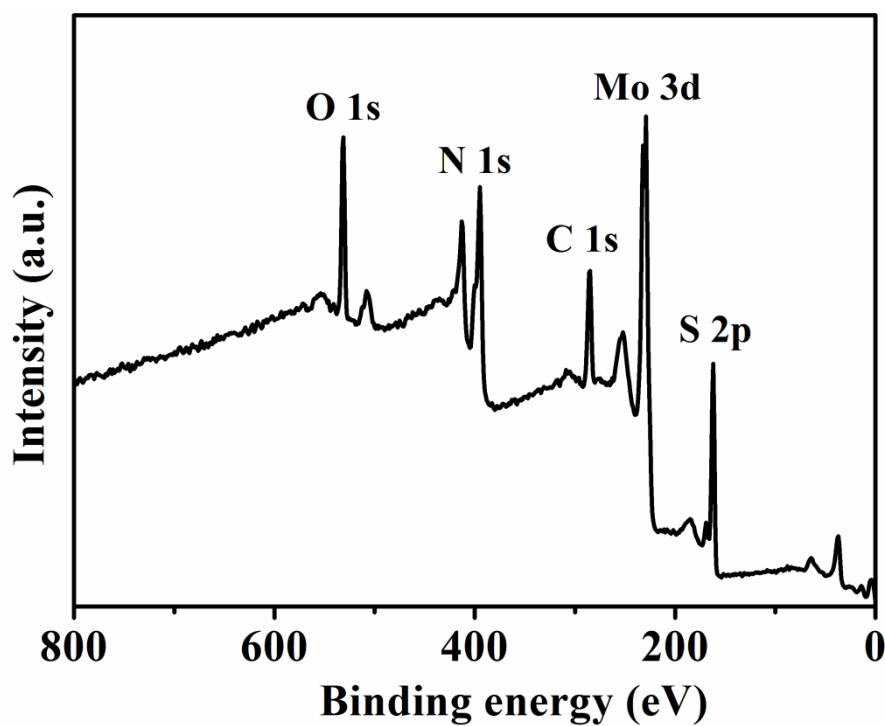


Fig. S6 XPS survey spectrum of PCN@MoS₂@C.

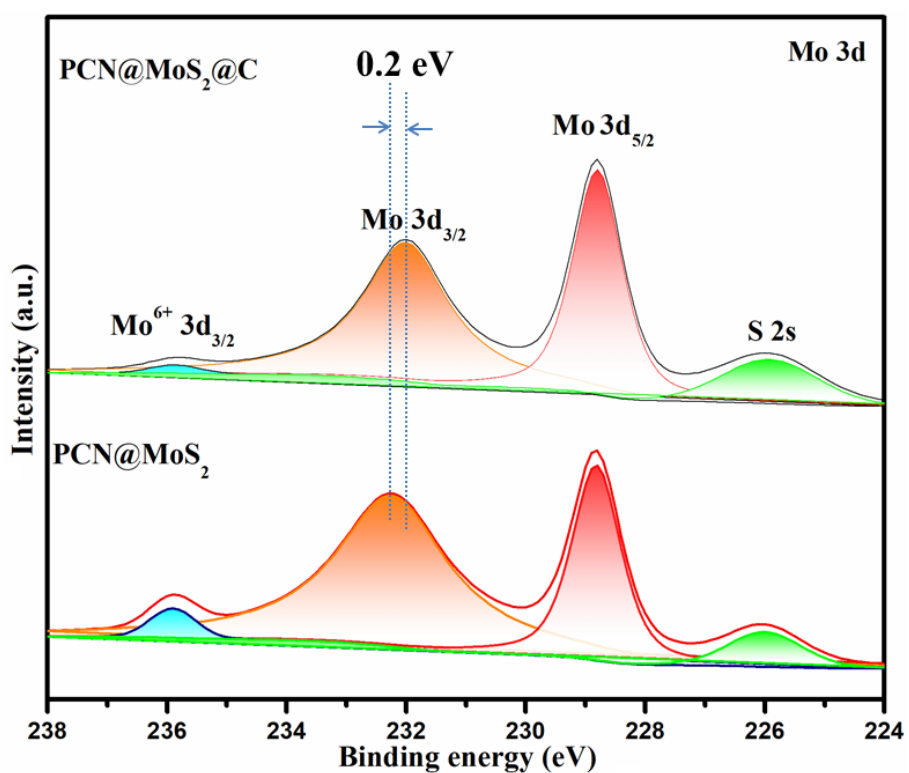


Fig. S7 The comparison of Mo 3d XPS spectra for PCN@MoS₂@C and PCN@MoS₂.

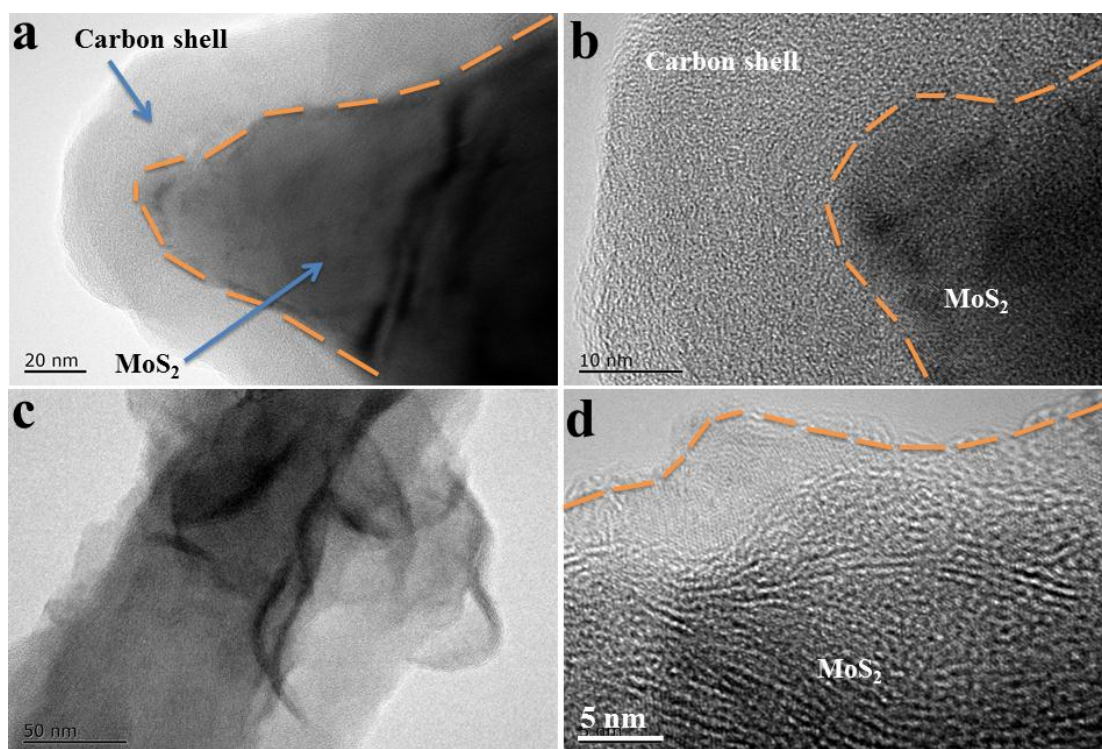


Fig. S8 (a, b) TEM and (c,d) HRTEM images of PCN@MoS₂@C with different thicknesses of carbon shells.

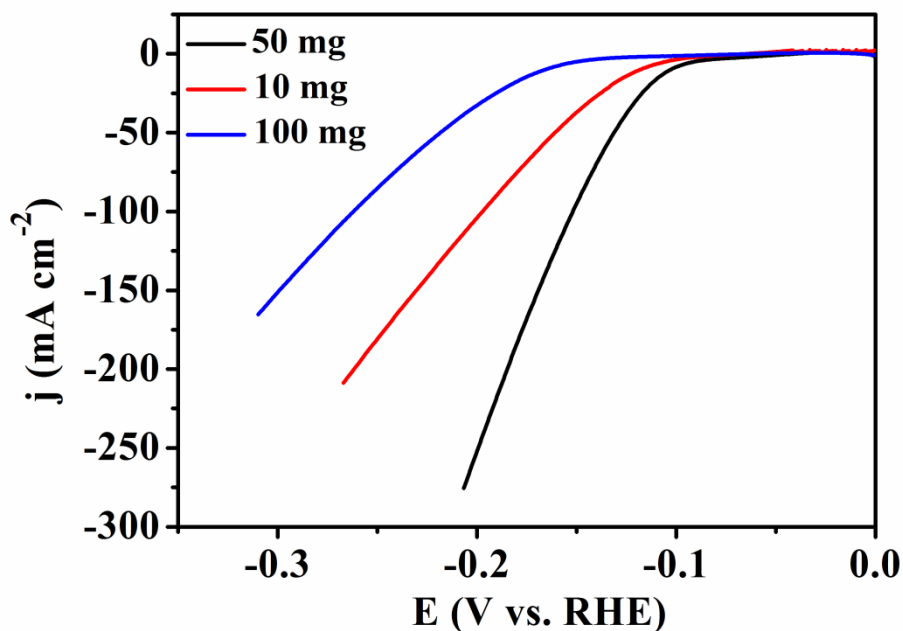


Fig. S9 The HER polarization curves of PCN@MoS₂@C samples with different thickness of carbon shells in 0.5 M H₂SO₄ solution (It should be noted that the HER activity of PCN@MoS₂@C is greatly dependent on the thickness of carbon shell. Another two samples with thinner or thicker carbon shells were prepared by changing the concentration of glucose (the carbon source of carbon shell). When a higher amount of glucose (100 mg) is used, MoS₂ nanosheets are tightly covered by carbon shell and the thickness of the carbon shell is up to 20 nm, much higher than that of PCN@MoS₂@C obtained from the reaction with 50 mg of glucose (Fig. S8). In contrast, only a small portion of MoS₂ nanosheets are covered by carbon shell and the thickness is only 1~2 nm if 10 mg of glucose was added. Both samples show inferior HER activity. As for the former sample, a too thick carbon shell covered on MoS₂ nanosheets can go against the electron transfer between catalyst and carbon shell, and block the active sites. As for the latter one, the heterostructure with a small amount of carbon shell may fail to provide sufficient conductivity and increase the number of active sites. Consequently, PCN@MoS₂@C with a carbon thickness of 2~4 nm was used as the catalyst in the following studies.)

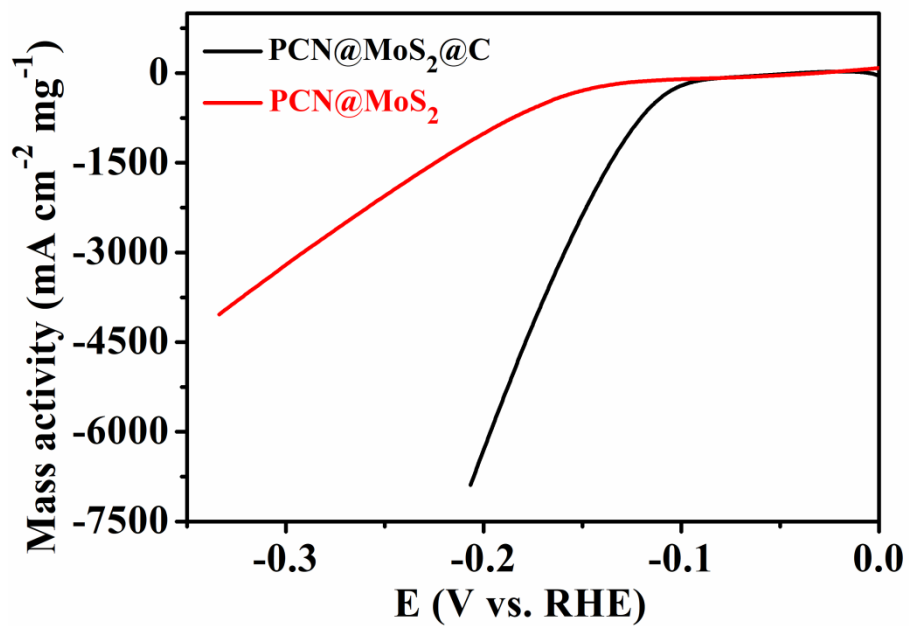


Fig. S10 The mass activity of each catalyst in 0.5 M H₂SO₄ solution.

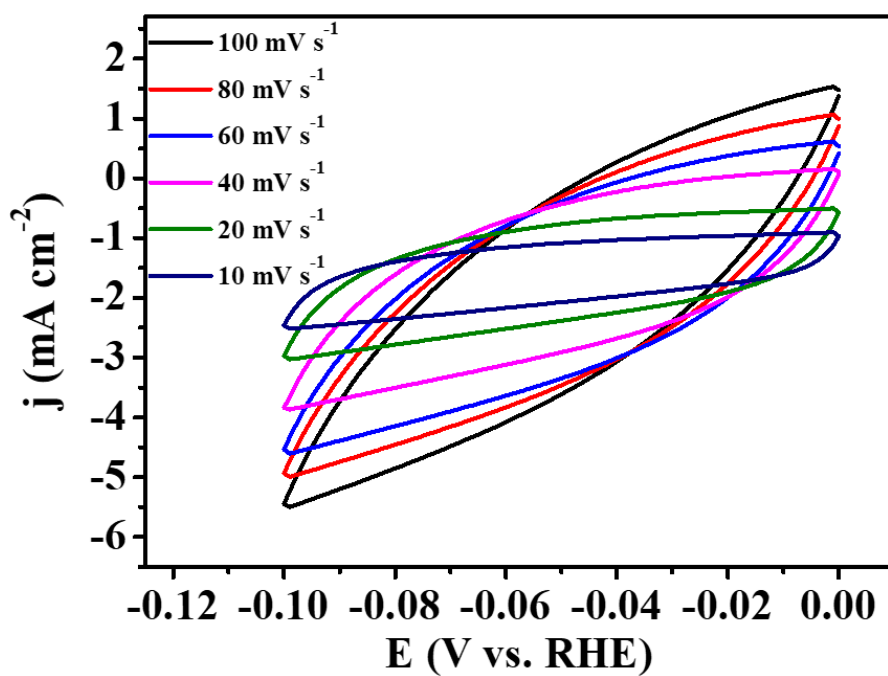


Fig. S11 CV curves of PCN@MoS₂@C at different scan rates.

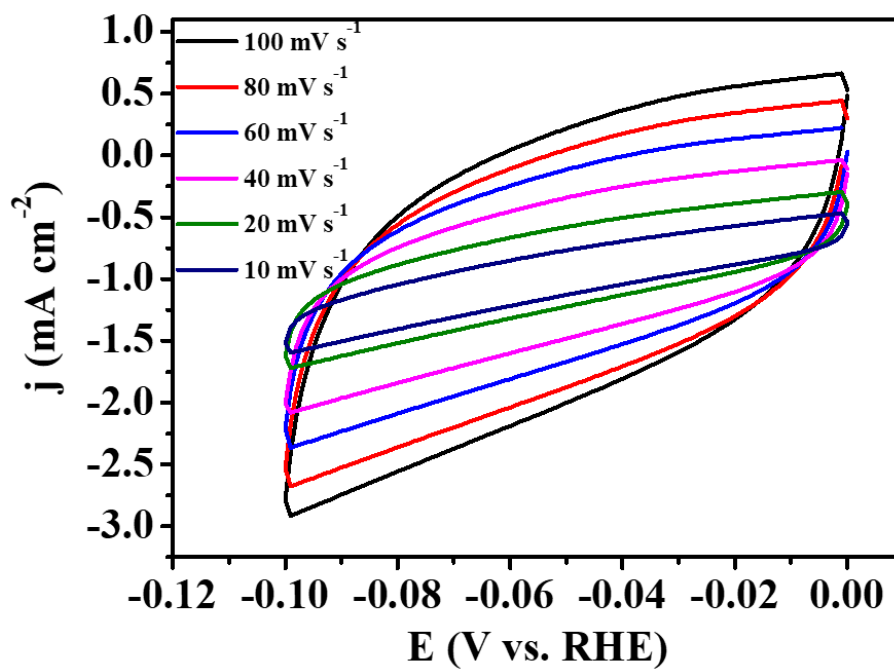


Fig. S12 CV curves of PCN@MoS₂ at different scan rates.

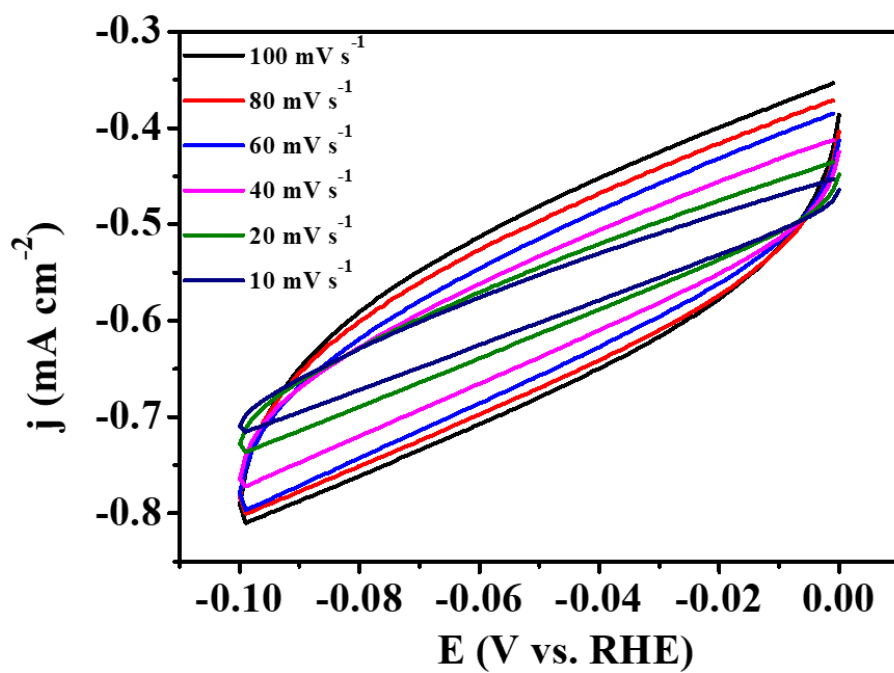


Fig. S13 CV curves of PCN at different scan rates.

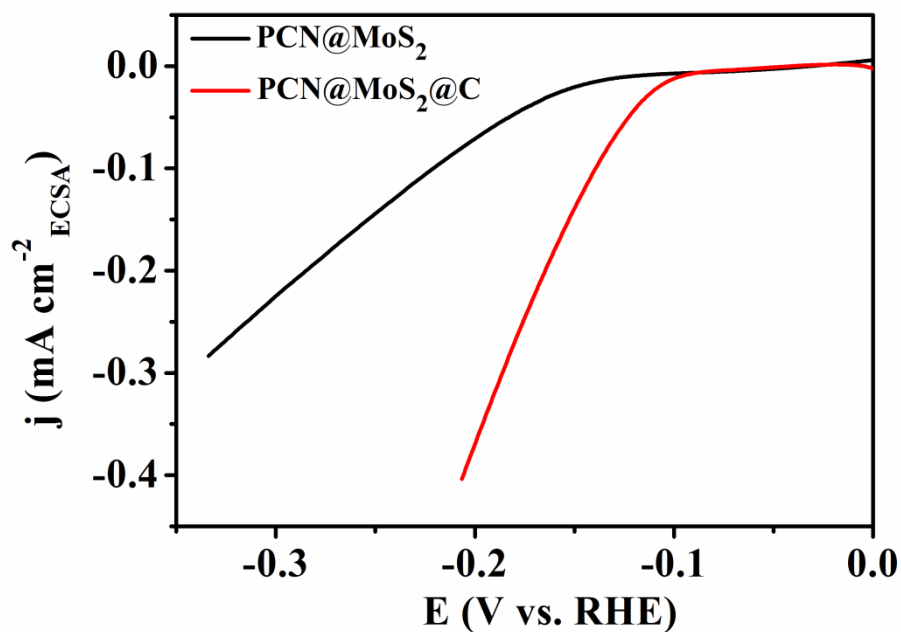


Fig. S14 The polarization curves of PCN@MoS₂@C and PCN@MoS₂ normalized by the ECSA.

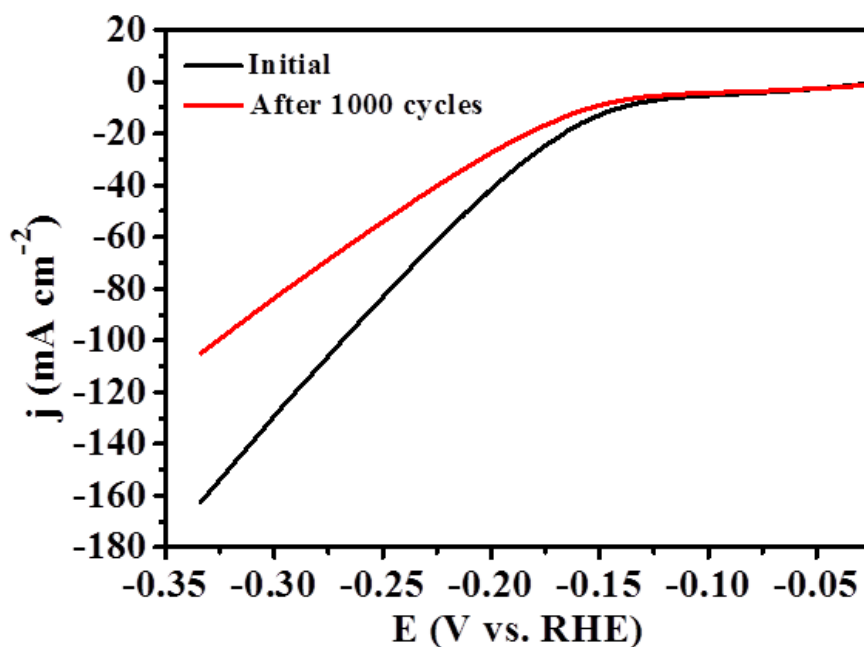


Fig. S15 The polarization curves of PCN@MoS₂ obtained initially and after 1000 CV cycles.

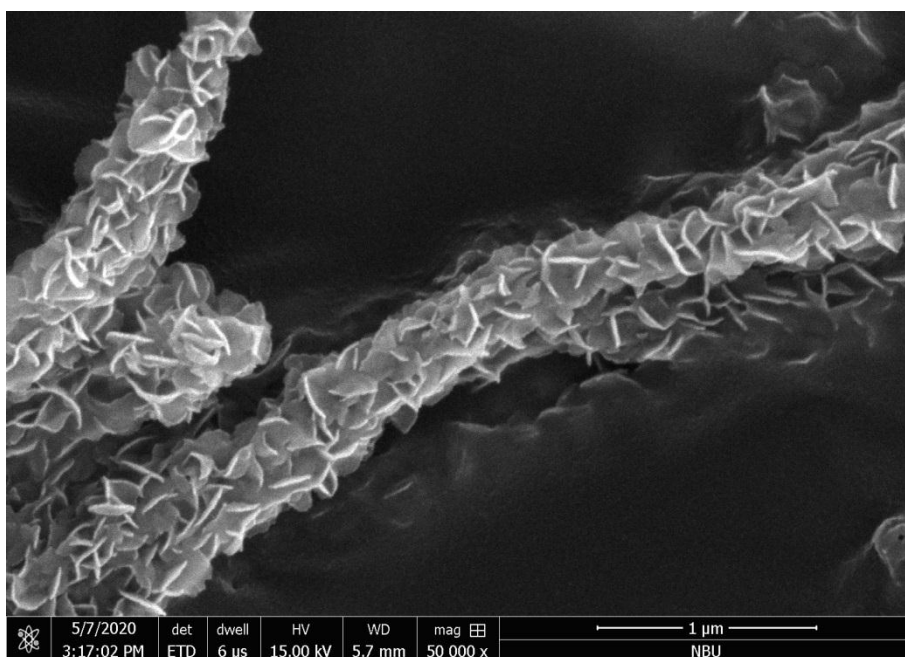


Fig. S16 The SEM image of PCN@MoS₂@C after long-term durability test.

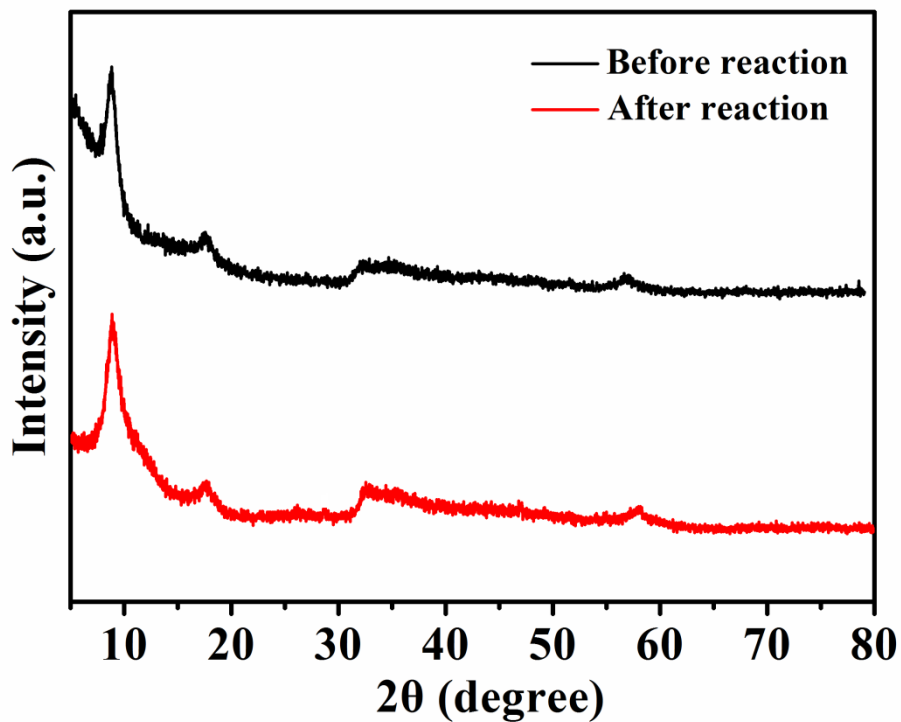


Fig. S17 The XRD patterns for PCN@MoS₂@C before and after long-term durability test.

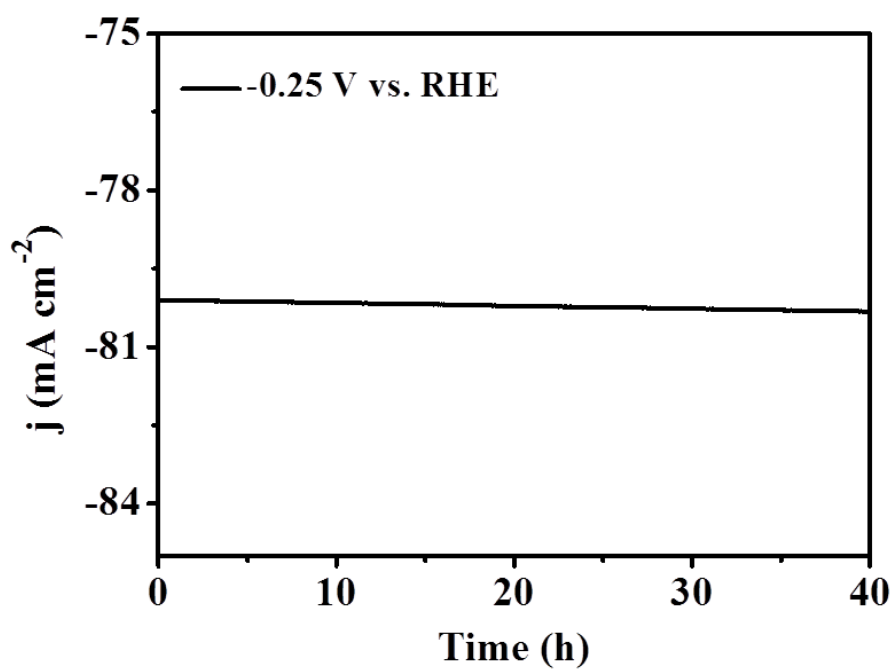


Fig. S18 The i - t plot of PCN@MoS₂@C at -0.25 V vs. RHE in 0.5 M H₂SO₄ solution.

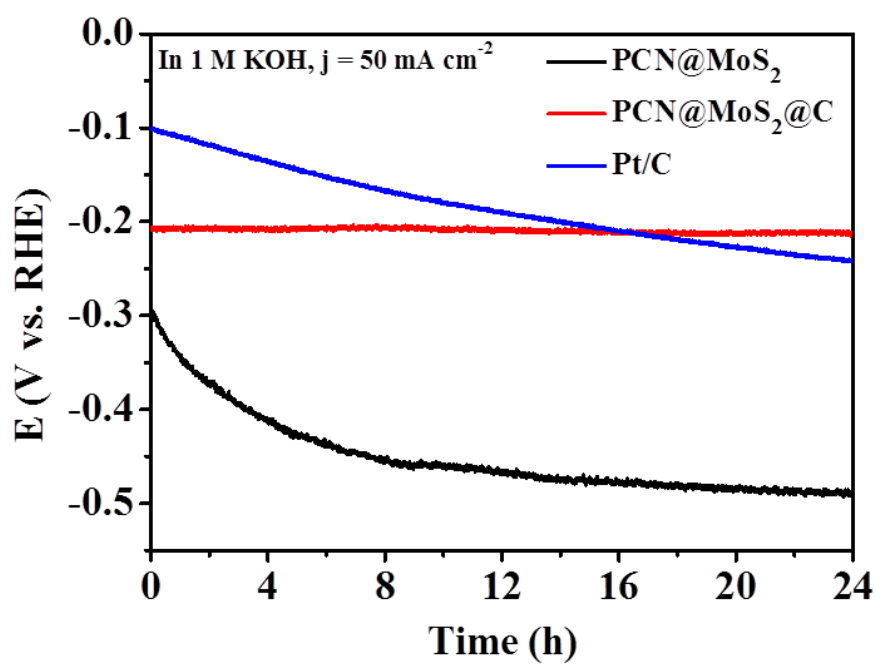


Fig. S19 Chronopotentiometric responses recorded on PCN@MoS₂, PCN@MoS₂@C and Pt/C at the current density of 50 mA cm⁻² in 1 M KOH solution.

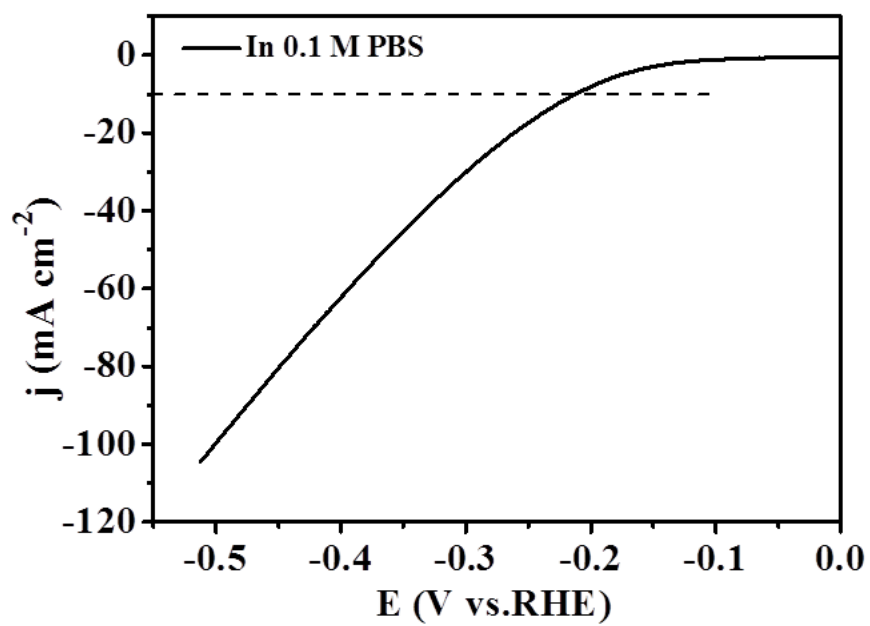


Fig. S20 The HER polarization curve of PCN@MoS₂@C in 0.1 M PBS.

Table S1. Comparison of the required overpotentials (η) to obtain the current density of 10 mA cm^{-2} and the Tafel slopes with recently reported MoS_2 based HER catalysts in $0.5 \text{ M H}_2\text{SO}_4$ solution.

Catalysts	η (mV) @ $j = 10$ mV cm^{-2}	Tafel slope (mV dec^{-1})	Ref.
PCN@ MoS_2 @C	130	50	This work
Defect-rich MoS_2	195	50	<i>Adv. Mater.</i> , 2013, 25 , 5807.
1T- MoS_2	187	43	<i>J. Am. Chem. Soc.</i> , 2013, 135 , 10274.
Amorphous MoS_x	160	40	<i>Acc. Chem. Res.</i> , 2014, 47 , 2671.
O-inncorporated MoS_2	190	55	<i>J. Am. Chem. Soc.</i> , 2013, 135 , 17881.
Co- MoS_3	171	56.9	<i>Adv. Mater.</i> , 2016, 28 , 92.
Strained vancy MoS_2	170	60	<i>Nat. Mater.</i> , 2016, 15 , 48.
Ni-Mo-S nanosheets	200	85.3	<i>Sci. Adv.</i> , 2015, 1 , e1500259.
Ni_{SA} - MoS_2	110	74	<i>Nano Energy</i> , 2018, 53 , 458.
MoS_2 /C HW	207	73	<i>J. Alloy. Compd.</i> , 2019, 777 , 514.
MoC/NPC@CNTs	175	62	<i>Sustainable Energy Fuels</i> , 2020, 4 , 407.

Table S2. Comparison of the required overpotentials (η) to obtain the current density of 10 mA cm^{-2} and the Tafel slopes with recently reported MoS_2 based HER catalysts in 1 M KOH solution.

Catalysts	η (mV) @ $j = 10$ mV cm^{-2}	Tafel slope (mV dec^{-1})	Ref.
PCN@ MoS_2 @C	150	67	This work
$\text{MoS}_2/\text{Ni}_3\text{S}_2$	110	83.1	<i>Angew. Chem. Int. Ed.</i> , 2016, 55 , 6701.
$\text{NiS}_2/\text{MoS}_2$ HNW	204	64	<i>ACS Catal.</i> , 2017, 7 , 6179.
	226	81	<i>Adv. Funct. Mater.</i> , 2016, 26 , 7386.
NiS-Ni(OH)_2 @ MoS_{2-x}			
CP/CTs/Co-S	131	190	<i>ACS Nano</i> , 2016, 10 , 2342.
Macroporous MoS_2 film	184	87	<i>Electrochim. Acta</i> , 2015, 168 , 133.
$\text{Ni}_2\text{P}/\text{MoO}_2$ @ MoS_2	226	81	<i>Nanoscale</i> , 2017, 9 , 17349.
$\text{MoO}_x/\text{Ni}_3\text{S}_2$	106	90	<i>Adv. Funct. Mater.</i> , 2016, 26 , 4839.